

Satellite observations reveal shorter periodic inner core oscillation

Yachong An^{1†}, Hao Ding^{1*}, Fred D. Richards², Weiping Jiang^{3*}, Jiancheng Li^{1*},

Wenbin Shen¹

¹*School of Geodesy and Geomatics, Hubei LuoJia Laboratory, Wuhan University, 430079, Wuhan, China*

²*Department of Earth Science & Engineering, Imperial College London, Royal School of Mines, Prince Consort Road, London, SW7 2AZ, UK*

³*GNSS Research Center, Wuhan University, Wuhan, China*

***Corresponding author. Email:** dhaosgg@sgg.whu.edu.cn; wpjiang@whu.edu.cn; jcli@sgg.whu.edu.cn

[†]Y.A. and H.D. contributed equally to this work.

Abstract: Detecting the Earth's inner core motions relative to the mantle presents a considerable challenge due to their indirect accessibility. Seismological observations initially provided evidence for differential/super-rotation of the inner core, but recently demonstrated a possibly ~70-year periodic oscillation. The contrasting results underscore the ongoing enigma surrounding inner core motion, leaving debates unresolved, including the precise oscillate period. In parallel to seismic observations, satellite geodesy has accumulated decades of global high-precision records, providing a novel avenue to probe inner core motions. Here, we detect an ~6-year oscillation from the gravitational field degree-2 order-2 Stokes coefficients derived from satellite observations, and find it has a unique phase correlation with the ~6-year signal in the

Earth's length-of-day variations. This correlation is attributed to an inner core oscillation which is controlled by the gravitational coupling between the inner core and lower mantle (mainly due to the density heterogeneity of the two large low-velocity provinces; LLVPs). That is, we independently corroborate the inner core periodic oscillation, albeit with a significantly shorter period than previously suggested. Our findings demonstrate the dense layer of the LLVPs (mean density anomalies of $\sim+9\%$ at the bottom), consistent with inversions from tidal tomography and Stoneley modes. Furthermore, our research reveals equatorial topographic undulations of 187 ± 4 m at the inner core boundary.

1. Introduction

The Earth's solid inner core and solid mantle are separated by the liquid outer core (Dziewonski & Anderson, 1991), and therefore the motions of the inner core are possible relative to the mantle. Both gravitational differentiation and early geodynamo simulations predicted a possible slight super-rotation of the inner core relative to the mantle (Gubbins, 1981). The initial evidence for this super-rotation, estimated at $\sim 1^\circ/\text{year}$, was provided by seismological observations (Song & Richards, 1996). However, subsequent analyses of seismic wave travel time and the free oscillation modes have presented a mixed picture, suggesting variations in the westward, eastward and westward, and even negligible differential rotation (Creager, 1997; Laske & Masters, 1999; Vidale et al., 2000; Tkalčić et al., 2013; Deuss, 2014). Recent seismological observations have tended towards the suggestion that the inner core may

undergo periodical oscillate relative to the mantle (Yang & Song, 2023; Wang & Vidale, 2022; Tkalčić, 2024). Such oscillation has the potential to reconcile the previously conflicting observations of differential rotation observed during seismic events. Despite this intriguing suggestion, robust evidence for periodic oscillation remains elusive, and proposed oscillation periods vary significantly across studies. An analysis comparing seismic wave observations at three time points (1969, 1971, 1974) with the length-of-day variation (ΔLOD) tried to confirm a possible ~ 6 -year inner core oscillation (Wang & Vidale, 2022). Another study leveraging a broader set of seismic events proposed a much longer ~ 70 -year oscillation period, with angular amplitudes reaching $\sim 1.5^\circ$, which are much higher than the period predicted by the dynamic model and the angular amplitude determined by free oscillation modes (Buffett, 1996; Laske & Masters, 1999); this is also considered as a trap of data selection in recent a study (Tkalčić, 2024). In addition, an alternative to explaining the travel time of seismic waves is the rapid growth of the inner core (Wen, 2006), throwing the detection results of the inner core from seismic waves into great uncertainty controversy.

Seismic tomography has revealed two mysterious anomalies in the lower mantle from the core-mantle boundary (CMB) to a height of ~ 1000 km known as the large low-velocity provinces (LLVPs), which present the degree-2 order-2 spherical harmonic $Y_{22}(\Omega)$ spatial structure, characterized by an equatorial antipodal configuration (Fig. 1; Conrad et al., 2013; Dehant et al., 2022). Despite some debate, LLVPs are considered as intrinsically dense heterogeneities due to a possible Moon-forming impactor (Koelemeijer et al., 2017; Lau et al., 2017; Richards et al., 2023; Yuan et al., 2023). If

this theory holds, the principal axis of the elliptical equator of the inner core will align with the principal axis of LLVPs due to the mantle-inner core gravitational (MICG) coupling (see as Fig. 1). A slight misalignment will trigger an inner core oscillation mode. Such oscillation mode can change the travel time of seismic waves (Song & Richards, 1996; Vidale et al., 2000), also cause the gravitational field degree-2 order-2 Stokes coefficient variations by driving changes in the Earth's degree-2 order-2 constant density surfaces (Buffett, 1996a; Dumberry & Manda, 2022), and change the ΔLOD through the angular momentum exchange with the mantle (Buffett, 1996a, b; Laske & Masters, 1999). Here, we will use the gravitational field Stokes coefficients derived from Satellite Laser Ranging (SRL) to independently identify periodic signals. We aim to correlate these signals with periodic variations in the ΔLOD to identify a possible inner core oscillation and determine its period and amplitude. The period and amplitude of the inner core oscillation can be further used to constrain the density anomalies of LLVPs and the equatorial topographic undulations of the inner core at the inner core boundary (ICB).

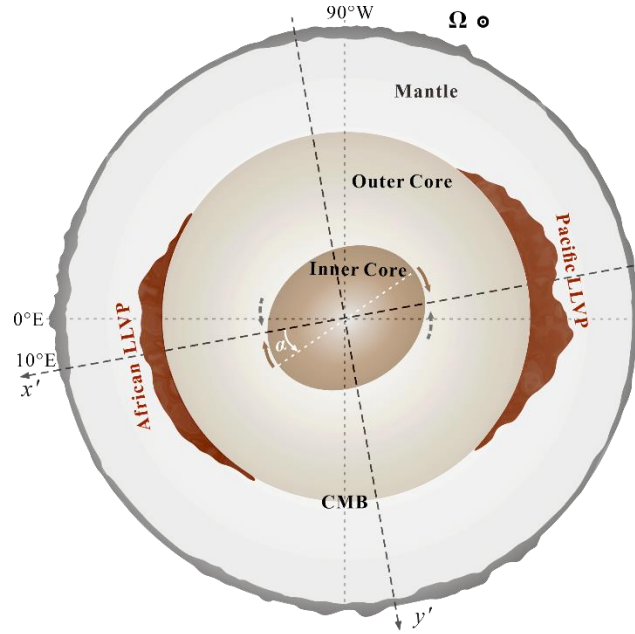


Fig. 1: Inner core oscillation diagram (view from the north pole). The inner core oscillation is a periodic reversal relative to the mantle. The dashed black line is set to the x' -axis in the right-handed coordinate system, representing the principal axis of the LLVPs (10°E - 170°W) at the lower mantle. If the density anomalies of the LLVPs are positive, the principal axis of the inner core (dashed white line) will be preferentially aligned with the principal axis of the LLVPs rather than the mantle's figure axis due to stronger gravity. The angle from the principal axis of the LLVPs to the inner core is α due to inner core oscillation.

2. Results

2.1 The angle between the principal axes of the large low-velocity provinces and the inner core

The principal axis of the LLVPs points to $\sim 10^\circ\text{E}$ - 10°W as shown in Fig. 1 (Dehant et al., 2022); the inner core will oscillate about this axis if the MICG coupling dominates the physical mechanisms and will change the ΔLOD due to the angular momentum exchange, so the angle between the principal axes of the LLVPs and the inner core can be inferred from the ΔLOD . The fluctuations in the ΔLOD (1962/1-2020/2) were

meticulously corrected using external sources (atmospheric and oceanic effects; Supplementary Fig. 1a), and the hydrological effect is not further considered due to it is far below even the background noise of ΔLOD in the target frequency band (Supplementary Fig. 1b). Subsequent removal of tidal effects based on a tidal model (Ray & Erofeeva, 2014), a corrected ΔLOD sequence $g_1(t)$ can be obtained (Fig. 2a); and after further employing a 6-month running mean to reduce significant high-frequency noises in the $g_1(t)$, a smoothed ΔLOD sequence $g_2(t)$ is obtained $g_2(t)$ (Fig. 2b). The $g_2(t)$ sequence consists of decennial variations and intradecadal (5-year to 10-year) oscillations with an amplitude of ~ 0.2 ms. Given that the intradecadal variations may be caused by possible inner core motions (Holme & De Viron, 2013; Mound & Buffett, 2003; Gross, 2007) while the decadal variations may be caused by fluid core motions (Braginsky, 1998, 1999; Buffett, 2014), fluctuations longer than 10-year are fitted and removed using the cosine function and the previously found periods (Ding, 2019) to obtain a final used residual sequence $R(t)$; this process is like that used in (Holme & De Viron, 2013). Given the assumption that the $R(t)$ primarily reflects the inner core motion, we can infer the angle α from the principal axes of LLVPs to the inner core, and generating $\varphi(t)$ sequences (Fig. 2b) from $R(t)$ (see Methods).

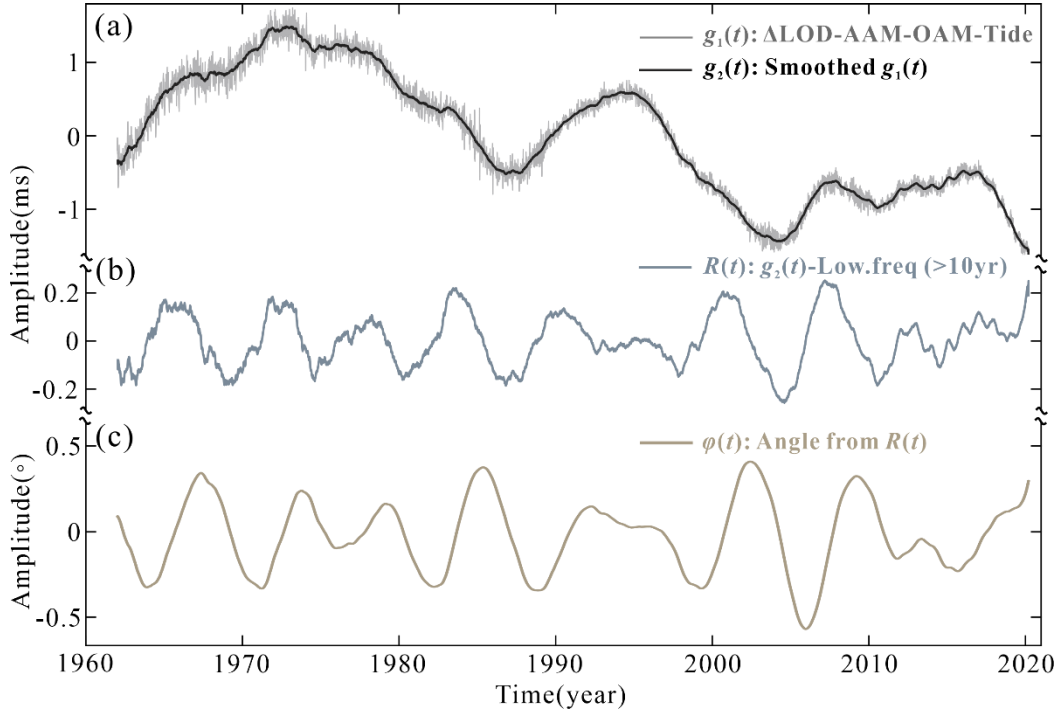


Fig. 2: Angle α from the principal axes of the large low-velocity provinces to inner core inferred from length-of-day variation (Δ LOD) time series. (a) The Δ LOD record with atmospheric and oceanic effects and tide removed ($g_1(t)$ sequences) and smoothed $g_1(t)$ sequences with a 6-month running mean window ($g_2(t)$ sequences). (b) Residual sequence $R(t)$ in which low-frequency signals with a period of more than 10-year are removed from $g_2(t)$ sequences. (c) Angle progression $\varphi(t)$ inferred from $R(t)$.

2.2. Searching for the inner core oscillation from the satellite determined Stokes coefficients

Under the mechanism depicted in Fig. 1, the inner core oscillation will also cause variations in the Earth's gravitational field, controlled by the heterogeneous LLVPs of the $Y_{22}(\Omega)$ spatial configuration (also known as quadrupoles). Thus, it is most likely to detect the inner core oscillation from the Stokes coefficient variations ΔC_{22} and ΔS_{22} (see Methods). ΔC_{22} and ΔS_{22} sequences (2002/1-2024/1) determined by SLR (satellite laser ranging) from CSR (recognized products) are firstly corrected using external

sources (atmospheric, oceanic, and hydrological effects; AOH effects). Theory predicts that the inner core oscillation can generally cause only observable ΔS_{22} and would not be detected in ΔC_{22} if the LLVPs have the high positive density anomalies as suggested in previous researches (Lau et al., 2017; Richards et al., 2023; Yuan, 2023) (see Methods). Consequently, we first compare the Fourier power spectra of the ΔC_{22} and ΔS_{22} sequences (Fig. 3a). In the period range of above 2-year, there is only a significant peak corresponding to a ~ 6 -year signal in the spectrum of the ΔS_{22} sequence (Fig. 3a). In contrast to ΔS_{22} , there is a significant spectral peak in the period range of 12-20 years in ΔC_{22} , and a much weaker spectral peak with ~ 5.3 -year period also presents in ΔC_{22} . As the length of the used ΔC_{22} is only 22 years, this spectral peak in the period of 12-20-year is probably not a stationary signal. Given that Fourier spectra are susceptible to non-stationary signals and thus to false results, we re-analyzed these two sequences in Fig. 3b by using the stabilized AR-z methods; this method helps to identify stationary harmonics (Ding et al., 2019) and has higher frequency resolution than Fourier spectra (Ding et al., 2018). Fig. 3b clearly shows a robust ~ 6 -year signal in ΔS_{22} but no corresponding signal in ΔC_{22} , which matches the identifying characteristics of the inner core oscillation. Besides, no significant spectral peak in the period of 12-20 years, which means that the spectral peak in the period of 12-20-year identified in Fig. 3a is not a stationary signal. To verify those results, we also show the Morlet wavelet spectra of the used $\Delta S_{22}/\Delta C_{22}$ after removing the AOH effects (Supplementary Fig. 2); results also show that the ~ 6 -year signal is only present in ΔS_{22} , and limited by period-resolution of the Morlet wavelet spectrum, the 12-20 years oscillation still presents in

ΔC_{22} but without a near-fixed period. Additionally, detailed Fourier power spectra of raw data and external excitations for $\Delta C_{22}/\Delta S_{22}$ are presented in Supplementary Fig. 3. The fluctuations observed within the 12-20 year and ~ 5.3 -year periods appear to be influenced by the AOH effects, whereas the ~ 6 -year signal evidently does not stem from these effects (Supplementary Fig. 3). Based on these results, only a ~ 6 -year signal is the candidate for inner core oscillation, and we refer it as to the SYO (\sim six-year oscillation). Subsequently, employing the classical least-squares method, we respectively fit the SYOs from ΔS_{22} and the $\varphi(t)$. As Fig 3c shows, the two fitted SYOs demonstrate nearly perfect synchronization. This finding aligns with the theoretical prediction $\Delta S_{22} = \mu \alpha$ (α in $^\circ$; see Methods), where $\mu = 8.237 \times 10^{-10} \xi_s > 0$ (ξ_s is a positive triaxiality parameter of the inner core) is obtained from parameters of PREM model. Based on the observed μ of $(5.2 \pm 0.1) \times 10^{-11}$ (derived from Fig. 3c), we estimate the triaxiality parameter ξ_s to be $(6.31 \pm 0.12) \times 10^{-2}$, which is close to the higher value of $\sim 6.69 \times 10^{-2}$ (i.e., the difference in equatorial moments of inertia $B_s - A_s = 9.51 \times 10^{30}$ kg·m²) in Buffett (1996a) inferred from a seismic tomography model of mantle based on hydrostatic equilibrium (Forte et al., 1994). This consistency strongly supports the assertion that the SYO is just the inner core oscillation. Additionally, the triaxiality parameter ξ_s implies the equatorial topographic undulations of 187 ± 4 m at the ICB.

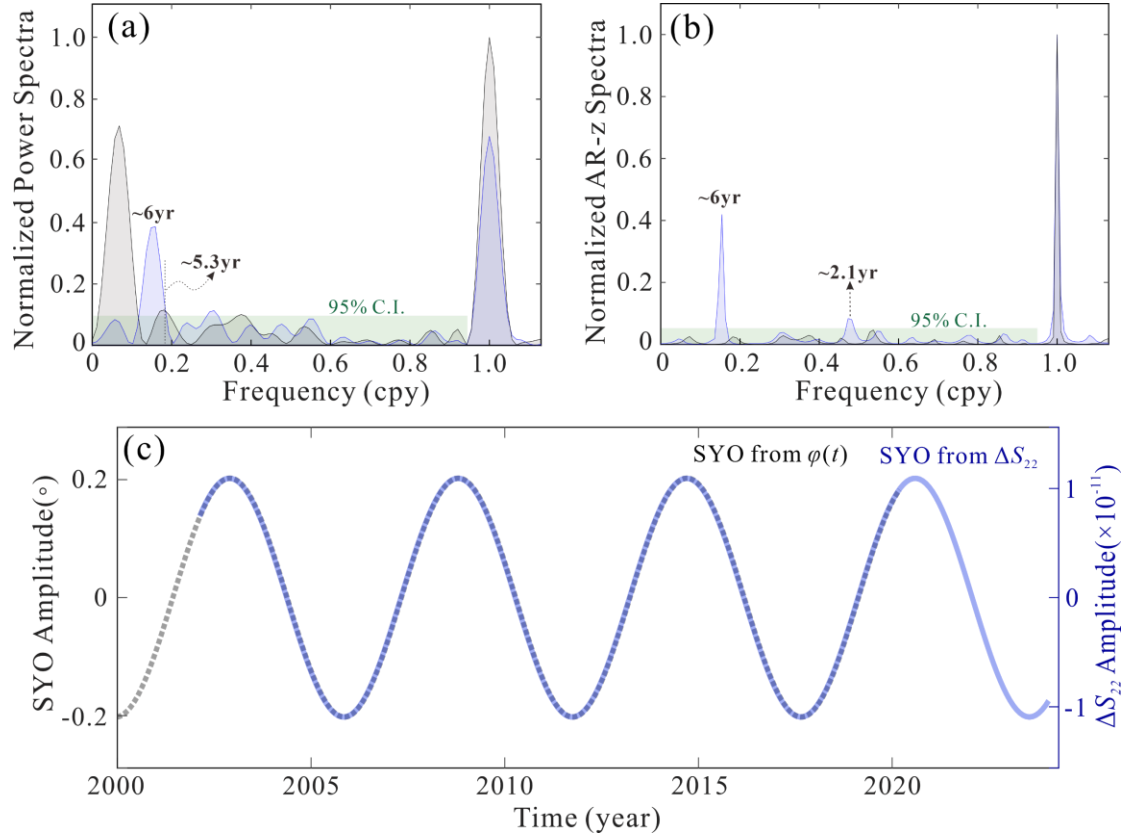


Fig. 3: Verification of the ~6-year oscillation (SYO) for the inner core oscillation from the length-of-day variation (ΔLOD) and degree-2 order-2 Stokes coefficients. (a) The normalized Fourier power spectra of the corrected degree-2 order-2 Stokes coefficient variations ΔC_{22} and ΔS_{22} sequences (2002/1-2024/1) determined by SLR; green region represents the 95% confidence interval (C.I.). (b) Similar to (a) but for the stable AR-z spectra. (c) Fitted SYOs from corrected ΔS_{22} sequences and angle $\varphi(t)$ using the classical least-squares method.

2.3 Inversion of the density anomalies of the large low-velocity provinces

According to the observed relationship between the ΔS_{22} and the inner core oscillation angle α , we have constrained the parameter ζ_s to the value of $(6.31 \pm 0.12) \times 10^{-2}$. Based on the estimated parameter ζ_s and ~6-year periodic inner core oscillation, it may yield important insights into the density anomalies of LLVPs in the

lower mantle.

Previous studies have shown that it requires an axial gravitational torque of $3 \times 10^{20} < \hat{\Gamma}_z < 4.5 \times 10^{20}$ N·m if the SYO is the normal mode of MICG oscillation with magnetic field (Mound & Buffett, 2003, 2006; Buffett & Mound, 2005; Holme & De Viron, 2013; Davies et al., 2014). Then, we obtain an important constraint from 1.59 to 2.48 for the mantle's density multipole of the interior type q_{22}^M (see Methods). The mantle's multipole of the interior type q_{22}^M can be regarded as weighted $p(a)$ integrals of the density anomaly $\varepsilon_{22}(a)$ of the bodies with spherical harmonic $Y_{22}(\Omega)$ spatial structure over the entire mantle. As depicted in Fig. 4a, the weight $p(a)$ -curve diminishes as the mean radius a increases, indicating a strong constraint on the degree-2 order-2 density anomaly in the lower mantle (blue and red dotted areas in Fig. 4b), corresponding to the highly heterogeneous and controversial density of the LLVPs for q_{22}^M . Thus, q_{22}^M can be used to constrain the density anomalies of the LLVPs.

Next, we use the constraint and the seismic shear wave speed (v_s) model of the mantle to invert the density anomalies of the LLVPs. The perturbation in shear wave speed v_s is converted perturbations in density ρ (i.e., density anomalies) by the $R_\rho = \partial \ln \rho / \partial \ln v_s$ (Karato, 1993; Lau et al., 2017). In the upper mantle and the middle and upper layers of the lower mantle (depth 0-1801 km), density anomalies are from the converted perturbations in seismic velocities based on the scaling factors from Karato (1993). In the middle and lower layers of the lower mantle (depth 1801-2891 km), different seismic tomographic models show that the LLVPs have similar long-wavelength structure (Lau et al., 2017), especially the spatial distribution of spherical

harmonic $Y_{22}(\Omega)$. Since the S40RTS (Ritsema et al., 2011) and S362MANI (Kustowski et al., 2008) models are sensitive to the LLVPs (Lau et al., 2017), we mainly adopted them to invert perturbations in density ρ . For the basalt in the deepest 100-200 km of the LLVPs, there may be a primitive chemical reservoir (Richards et al., 2023), as a constant R_ρ conversion is used from CMB to a depth of 2691 km. In the outermost layer of the LLVPs (depth 1801-2131 km), the density anomalies are obtained by setting $R_\rho = 0.2$ from Karato (1993) and Lau (2017). To smooth the transition of density to the upper and middle layers of the lower mantle, the R_ρ is varied linearly with depth from 2131 to 2691 km. The density anomalies of the LLVPs are obtained by adjusting R_ρ and applying crust correction based on the model CRUST1.0 (Laske et al., 2013) to meet the multipole constraint q_{22}^M . Fig. 4a shows the variation of the mean density anomalies with radius of the deep LLVPs below the radius and the contour of the LLVPs in each layer (see green curves in Fig. 4b) is defined by the $-6.5\%V_s$ (Karato et al., 1993; Lau et al., 2017; Richards et al., 2023) based on the S40RTS model (similar results based on the S362MANI model are shown in Supplementary Fig. 4). For the bottom two-thirds of the LLVPs, the mean density of our inversion is $+4.5\text{-}5.8\%$ higher than that of the surroundings based on the S40RTS model ($+4.7\text{-}6.1\%$ for S362MANI model), consistent with the independent result of $+5\%$ constrained by the tidal tomography (Lau et al., 2017). Fig. 4b show the density anomalies of the layer at the depth of 2851 km (40 km from the CMB; mean radius $a = 3520$ km) based on the constraint of density multipole $q_{22}^M = 2.16$ (corresponding to the axial gravitational torque of $\hat{\Gamma}_z = 4.0 \times 10^{20}$ N·m; Buffett & Mound, 2005) and S40RTS model; this indicates the very dense LLVPs

at the bottom with a mean density anomaly of about $\sim+9\%$, which is close to the independent result ($\sim+10\%$) of Stoneley mode splitting functions (Koelemeijer et al., 2017). These independent measurements corroborate each other and indicate that LLVPs have large positive density anomalies and that there may indeed be an abnormally dense layer at the bottom (Koelemeijer et al., 2017; Lau et al., 2017; Richards et al., 2023; Yuan et al., 2023). More importantly, these conformities in turn support ~ 6 -year signal for the inner core oscillation.

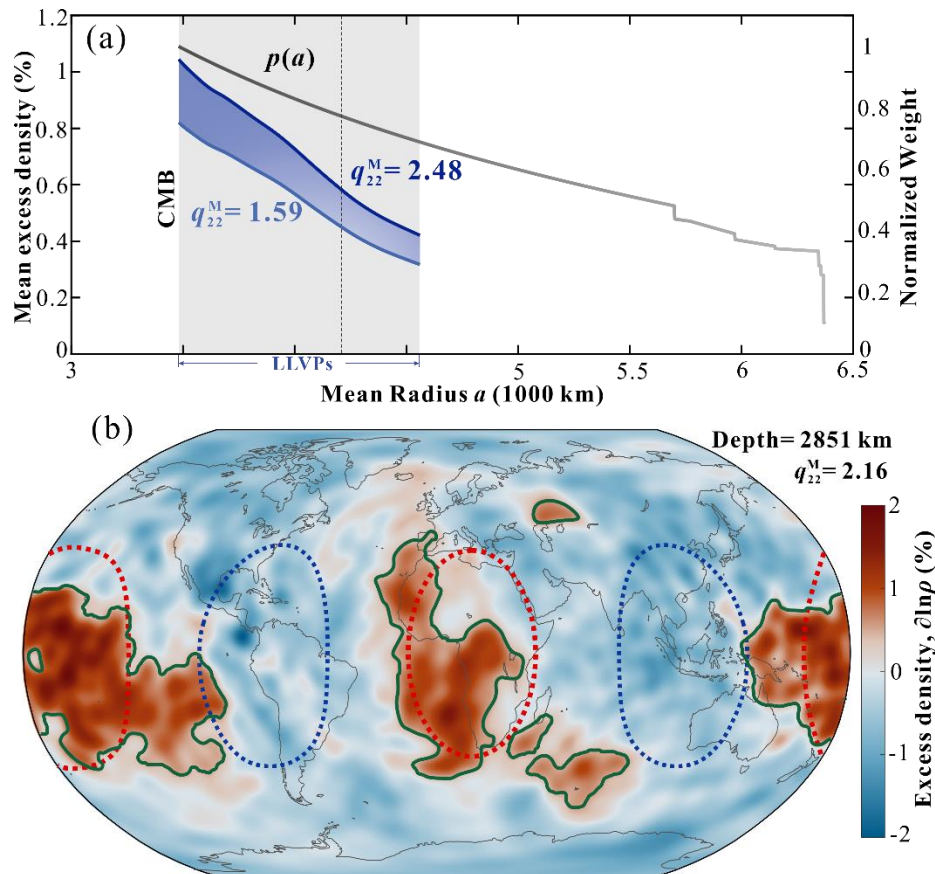


Fig. 4: Inversion of the density anomaly of the large low-velocity provinces (LLVPs) based on S40RTS model. (a) Normalized weight function $p(a)$ (gray curve) and the mean radius-dependent mean density anomaly range of the LLVPs below the radius (blue shaded area); the gray shaded area indicates the LLVPs location range. (b) The excess density $\delta \ln \rho$ (in %) converted by the S40RTS model at the depth of 2851 km is based on the mantle's interior multipole value of 2.16 (corresponding to the axial

gravitational torque of 4.0×10^{20} N·m; Buffett & Mound, 2005); the green curves circle the contour of the LLVPs defined by the $-6.5\% V_s$ (Karato et al., 1993; Lau et al., 2017; Richards et al., 2023); the dashed curves circle the sensitive region of degree-2 order-2 density multipoles and different colors mean that they have opposite symbols.

4. Discussion and Conclusion

Growing evidence suggests that the equatorial plane of the inner core is an ellipse (Forte et al., 1994; Buffett, 1996a; Zhang & Shen, 2020) shaped by lateral differences in the lowermost mantle density due to the LLVPs. On this premise, if the inner core has a stable super-rotation, periodic oscillation is almost impossible because its physical mechanism will breakdown soon unless a low-viscosity inner core (the inner core can deform viscously; Buffett, 1997). However, different observations have shown that inner core oscillation is not only possible but also persistent, potentially driven by gravitational coupling between the inner core and the LLVPs in the lower mantle (Buffett, 1996a; Mound & Buffett, 2003, 2006; Buffett & Mound, 2005; Chao, 2017). While seismology provides a traditional means of probing the inner core motions, it suffers from limitations such as sparse seismic events coverage (Song & Richards, 1996; Yang & Song, 2023; Wang & Vidale, 2022; Tkalčić, 2024) and ambiguity in interpreting different travel times of seismic waves (Wen, 2006). In contrast, to verify the existence of inner core oscillation (and determine its period), we use high-precision low-degree satellite gravitational field data as an additional observational constraint, which has high temporal resolution (monthly sampling) and reflects the overall change of the inner core's equator that it can avoid a trap of data selection (Tkalčić, 2024) and the influence

of the rapid growth of the inner core in seismology (Wen, 2006). Based on the gravitational coupling between the inner core and LLVPs in the lower mantle, the inner core oscillation only occurs theoretically in the gravitational field coefficient ΔS_{22} and not in ΔC_{22} . Our measured data results also demonstrate that a ~ 6 -year signal appears only in ΔS_{22} and hence confirms the theoretical prediction. Correspondingly, there is also an SYO in the ΔLOD . Since the signal in the ΔLOD is caused by the exchange of angular momentum between Earth's different layers, after excluding possible external sources, it is currently considered to be most likely to originate from inner core oscillation. Furthermore, the SYO in ΔS_{22} corresponds well in phase to that in the inner core differential rotation angle inferred from ΔLOD (this is also consistent with the verification based on seismic waves in Wang & Vidale (2022)). This finding further confirms that the SYO is from inner core oscillation and that the gravitation coupling between the inner core and LLVPs plays a key role in its mechanism. Integrating observations from satellite geodesy with theoretical analysis, we inverted the triaxiality of the inner core of $(6.31 \pm 0.12) \times 10^{-2}$; this means that the inner core's equatorial topographic undulations of 187 ± 4 m and the difference in equatorial inertia moments $B_s - A_s$ of $(8.972 \pm 0.172) \times 10^{30}$ kg·m², which is close to the high value inferred from seismic tomography (Forte et al., 1994; Buffett, 1996a). Although the magnetic field in the fluid core would result in a smaller oscillation angle of the inner core, the standing wave formed in the liquid core would further perturb the global gravitational field and would not be expected to significantly alter those results. Based on the mechanism of the gravitation coupling between the inner core and LLVPs and considering the

magnetic field of the core, we inverted very dense LLVPs at the bottom with a mean density anomaly of about $\sim+9\%$, and the bottom two-thirds of the two LLVPs with the mean density anomaly of $+4.5-5.8\%$, which agree with independent measurements from tidal tomography and Stoneley mode splitting function (Koelemeijer et al., 2017; Lau et al., 2017; Richards et al., 2023), respectively. This coherence across multiple lines of observed evidence not only strengthens the argument for the proposed mechanism of ~ 6 -year inner core oscillation but also underscores the intricate interplay between Earth's inner core, magnetic field, and mantle dynamics. Collectively, these findings from satellite geodesy make contribute significantly to our comprehension of the Earth's inner structure and the dynamic processes governing its behavior.

Methods and Supplementary Information

for Satellite observations reveal shorter periodic inner core oscillation

1. Methods

Inferring the angle α from the length-of-day variation

In the MICG coupling system, the relationship between the mantle angular velocity variation $\Delta\omega_m$ and the inner core angular velocity variation $\Delta\omega_s$ is established through

$$\Delta\omega_s C_s = -\Delta\omega_m C_m \quad (1)$$

where C_s and C_m are the axial inertia moments of the inner core and mantle, respectively.

The angular velocity variation of the mantle can be obtained from the observed ΔLOD

by

$$-\frac{\Delta\omega_m}{\Omega_0} = \frac{\Delta\text{LOD}}{\text{LOD}} \quad (2)$$

where $\text{LOD} = 86400$ s, and Ω_0 denotes the mean sidereal rotation rate. The rotated angle of the mantle in the opposite direction is negligible compared to the rotated angle of the inner core, and the angle α is

$$\alpha = \int \Delta\omega_s dt \quad (3)$$

Eqs. (1)-(3) yield the final expression of the angle α

$$\alpha = \frac{C_m}{C_s} \frac{\Omega_0}{\text{LOD}} \int \Delta\text{LOD} dt \quad (4)$$

In inverting the angle α , we assume that the ΔLOD is caused by the inner core oscillation or super-rotation, which is valid for a certain frequency band.

Changes in Stokes coefficients caused by the inner core oscillation

The inner core oscillation causes the misalignment of the mantle and inner core in the equatorial plane, which is associated with degree-2 order-2 ellipticity and further causes a change in the Earth's gravity field. Thus, only the degree-2 order-2 ellipticity of the Earth needs to be considered, and constant density surfaces of Earth are written as (Buffett, 1996a)

$$r' = a(1 + \epsilon' Y_{22} + \epsilon'^* Y_{2-2}) \quad (5)$$

where $\epsilon' = \epsilon'(a)$ denotes the equatorial ellipticity varying with mean radius a , the asterisk ‘*’ represents complex conjugation, and $Y_{22} = Y_{22}(\theta, \varphi)$ is degree-2 order-2 fully normalized spherical harmonic function. Given that selected x' -axis aligns with the principal axes of the inner core and LLVPs in static equilibrium, the ellipticity ϵ' can be

approximated as a real number.

The inner core oscillation only involves rotation in the equatorial direction. Following an equatorial rotation in the longitudinal direction α , as shown in Fig. 1, the elastic displacement in constant density surfaces of inner core caused by the misalignment of the inner core is

$$\Delta \hat{r}_s = \hat{r}_s - r' = (1 + h_{\epsilon'}) (\tilde{r}_s' - r_s') = \sum_{m=-2}^2 \gamma_{\alpha}^m a \epsilon' (1 + h_{\epsilon'}) Y_{2m} \quad (6)$$

where

$$\begin{aligned} r_{\alpha}^0 &= r_{\alpha}^{\pm 1} = 0 \\ r_{\alpha}^{\pm 2} &= e^{\mp i 2 \alpha} - 1 = \mp i 2 \alpha \end{aligned} \quad (7)$$

Similar to the inner core wobble, we only need to replace the ellipticity ϵ and $\delta_{\beta\alpha}^m$ in Dumberry (2008) with ϵ' and γ_{α}^m , respectively, to derive the conclusion regarding inner core oscillation. Thus, the change in the surface's gravitational field caused by the elastically misaligned inner core is

$$\Delta U(a_e, \theta, \lambda) = G \sum_{m=-2}^2 \gamma_{\alpha}^m \sqrt{\frac{4\pi}{5}} \frac{1}{a_e^3} (\mathcal{H}_s - \mathcal{H}_s') [1 + \tilde{k}_{\epsilon'}(a_e)] Y_{2m} \quad (8)$$

where $G = 6.672 \times 10^{-11} \text{ N}\cdot\text{m}^2\cdot\text{kg}^{-2}$ denotes gravitational constant, $a_e = 6.371 \times 10^6 \text{ m}$ represents the mean radius of the Earth, and the factor $[1 + \tilde{k}_{\epsilon'}(a_e)] = 1.9736$ accounts for the Earth's elastic deformations associated with the density change at the ICB and is written as (Dumberry, 2008)

$$\tilde{k}_{\epsilon'}(a_e) = \frac{\mathcal{H}^{\epsilon'}}{(\mathcal{H}_s - \mathcal{H}_s')} \quad (9)$$

Those three parameters related to equatorial ellipticity are defined as

$$\mathcal{H}_s = -\sqrt{\frac{4\pi}{5}} \int_0^{a_s} \rho \frac{d(a^5 \epsilon')}{da} da \quad (10a)$$

$$\mathcal{H}_s' = -\sqrt{\frac{4\pi}{5}} \int_0^{a_s} \rho_f' \frac{d(a^5 \epsilon')}{da} da \quad (10b)$$

$$\mathcal{H}^{\epsilon'} = -\sqrt{\frac{4\pi}{5}} \int_0^{a_s} \rho \frac{d(a^5 h_{\epsilon} \epsilon')}{da} da \quad (10c)$$

where $a_s = 1.2215 \times 10^6$ m denotes the mean radius of the ICB (inner core boundary).

The triaxiality parameter of the inner core is also used here, and it is defined as

$$\xi_s = \frac{B_s - A_s}{C_s - \frac{A_s + B_s}{2}} = -4 \sqrt{\frac{1}{6}} \int_0^{a_s} \rho \frac{d(a^5 \epsilon')}{da} da / \int_0^{a_s} \rho \frac{d(a^5 \epsilon)}{da} da \quad (11)$$

where $C_s = 5.8673 \times 10^{34}$ kg·m², B_s , and A_s denote the principal moments of inertia of the inner core, respectively, arranged in descending order. Since the inner core's density changes very little (only ~2.5% from the Earth's center to the ICB based on the PREM model; Dziewonski & Anderson, 1981), the two unknown quantities in Eqs. 10a and 10b are linked to the known quantities defined in Chao (2017) based on the triaxiality parameter,

$$\mathcal{H}_s = -\frac{\sqrt{6}}{4} \xi_s \mathcal{H}_s' \quad (12a)$$

$$\mathcal{H}_s' \approx -\frac{\sqrt{6}}{4} \xi_s \mathcal{H}_s \quad (12b)$$

The error introduced by the approximation of Eq. 12b is negligible, and can therefore be equated. Based on the PREM model (Dziewonski & Anderson, 1981), we can calculate the parameters $\mathcal{H}_s = 1.418 \times 10^{32}$ kg·m² and $\mathcal{H}_s' = 1.342 \times 10^{32}$ kg·m². The inner core oscillation only causes the degree-2 order-2 Stokes coefficient change, and considering the difference between geographic coordinate and set in this study, it is written as

$$\begin{aligned}\Delta C_{22} + i\Delta S_{22} &= i\sqrt{\frac{3}{5}} \frac{1}{Ma_e^2} \xi_s (\mathcal{H}_s - \mathcal{H}_s') [1 + \tilde{k}_{e'}(a_e)] e^{-i\frac{10^\circ}{180^\circ}\pi} \alpha \\ &\equiv (\nu + i\mu)\alpha\end{aligned}\quad (13)$$

If the density anomalies of the LLVPs are positive, it will be likely that the inner oscillation only causes the observable ΔS_{22} . Otherwise, it will cause observable changes in ΔC_{22} . Based on the above parameters, it can be calculated $\mu = 8.237 \times 10^{-10} \xi_s$ (where α is in $^\circ$).

The axial gravitational torsion constant and density multipoles

After determining the triaxiality parameter of the inner core, the density multipole of the mantle can be inverted utilizing the axial gravitational torsion constant, provided the SYO corresponds to the inner core oscillation. The axial gravitational torsion constant is mainly contributed by degree-2 order-2 density multipoles and is expressed as (Chao, 2017a, b)

$$\hat{\Gamma}_z = \frac{32\pi}{5} G\gamma f_s |q_{22}^M| |Q_{22}^s| \quad (14)$$

where the factor $\gamma = \Delta\rho/\rho_s = 0.0468$ accounts for the hydrostatic pressure effect of the passive outer core, and the factor $f_s = 0.85$ account for elastic deformation of the inner core oscillation (Chao, 2017a, b; Rochester et al., 2018). The degree-2 order-2 multipole of the interior type belonging to the mantle q_{22}^M and the exterior type belonging to the inner core Q_{22}^s are defined as (Chao, 2017a)

$$q_{22}^M = \iiint_{\text{Mantle}} \rho(\mathbf{r}) r^{-1} Y_{22}(\Omega) dr d\Omega \quad (15a)$$

$$Q_{22}^s = \iiint_{\text{IC}} \rho(\mathbf{r}) r^4 Y_{22}^*(\Omega) dr d\Omega \quad (15b)$$

respectively. An alternative idea to Eq. 5 is to consider the 3-D density of the Earth,

similarly focusing only on the degree-2 order-2 lateral variation of the Earth, the density is expressed as

$$\rho(r, \theta, \varphi) = \rho_{\text{Model}}(r) \left(1 + \varepsilon_{22} Y_{22} + \varepsilon_{22}^* Y_{2-2} \right) \quad (16)$$

where ε_{22} denotes the density anomaly coefficient of the spherical harmonic $Y_{22}(\theta, \varphi)$.

Using Eq. 16, Eqs. 15a and 15b can be re-written as

$$\begin{aligned} q_{22}^{\text{M}} &= \int_{a_f}^{a_e} \frac{\rho_{\text{Model}}(a) \varepsilon_{22}(a)}{a} da \\ &= \int_{a_f}^{a_e} p(a) \varepsilon_{22}(a) da \end{aligned} \quad (17a)$$

$$\begin{aligned} Q_{22}^s &= \int_0^{a_s} a^4 \rho_{\text{Model}}(a) \varepsilon_{22}^*(a) da \\ &= \sqrt{\frac{15}{32\pi}} (B_s - A_s) \exp(-2i\Lambda) \\ &= \sqrt{\frac{15}{32\pi}} \xi_s C_s e_s \exp(-2i\Lambda) \end{aligned} \quad (17b)$$

where $p(a)$ is defined as the weight function of density anomaly coefficient in the mantle, and we can discern what part q_{22}^{M} is sensitive to by analyzing the weight function $p(a)$ -curve in the mantle; Λ represents the angle between the direction of the minimum moment of inertia of the inner core A_s and the x -axis of geographical coordinate; $e_s = 2.422 \times 10^{-3}$ denotes the dynamical ellipticity of the inner core. By combining Eqs. 14 and 17b, we obtain the final relation

$$|q_{22}^{\text{M}}| = \sqrt{\frac{5}{96\pi}} \frac{\hat{\Gamma}_z}{G \gamma f_s \xi_s C_s e_s} \quad (18)$$

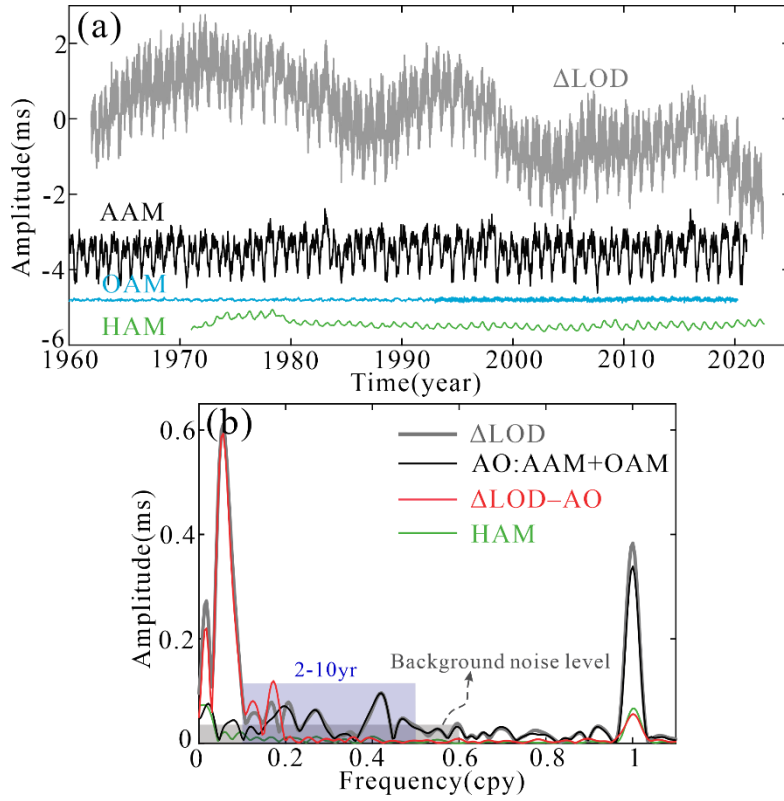
where the factor $\gamma = \Delta\rho/\rho_s = 0.0468$ accounts for the hydrostatic pressure effect of the passive outer core, and the factor $f_s = 0.85$ account for elastic deformation of the inner core oscillation (Chao, 2017a, b; Rochester et al., 2018). The degree-2 order-2 multipole of the interior type belonging to the mantle q_{22}^{M} and the exterior type

belonging to the inner core Q_{22}^s are defined as (Chao, 2017a)

2. Supplementary Information

Length-of-day variation observation and external excitation sources

The length-of-day variation (ΔLOD) observation spanning from 1962/1 to 2022/6, with daily sampling, are depicted in Supplementary Fig. 1, alongside the corresponding results excited by atmospheric angular momentum (AAM; spanning from 1948/1 to 2021/1, with 6-hour sampling), oceanic angular momentum (OAM; spanning from 1949/1 to 2020/2, with 10-day sampling), and hydrological angular momentum (HAM; spanning from 1971/1 to 2022/7, with daily sampling). Their respective Fourier amplitude spectra are presented in Supplementary Fig. 1b. Notably, within periods shorter than 5 years, the amplitude of ΔLOD observation and this excited by AAM and OAM exhibit remarkable similarity (illustrated by the black fine curve and gray thick curve, respectively). Subsequent removal of atmospheric and oceanic effects (denoted by the red curve) results in the elimination of nearly all signals, with residual noise closely resembling hydrological effects (as depicted by the green curve). Thus, signals with periods shorter than 5 years predominantly originate from external sources, and the candidate signal for the inner core oscillation is not in this band. Interestingly, upon removal of atmospheric and oceanic effects, signals on the intradecadal scale exhibit amplification (illustrated by the gray thick curve and red curve), while the contribution of hydrological effect remains significantly lower than background noise (as indicated by the green curve). Consequently, signals on the intradecadal scale primarily arise from the Earth's interior, representing a suspicious frequency band for investigating inner core oscillation. On a decade-scale or longer, although signals are attenuated following atmospheric and oceanic removal, background noise surpasses hydrological effect. Therefore, the possibility of inner core oscillation cannot be dismissed within this frequency band, prompting further investigation to exclude inner core oscillation through combined analysis of gravitational field observations and theoretical model.

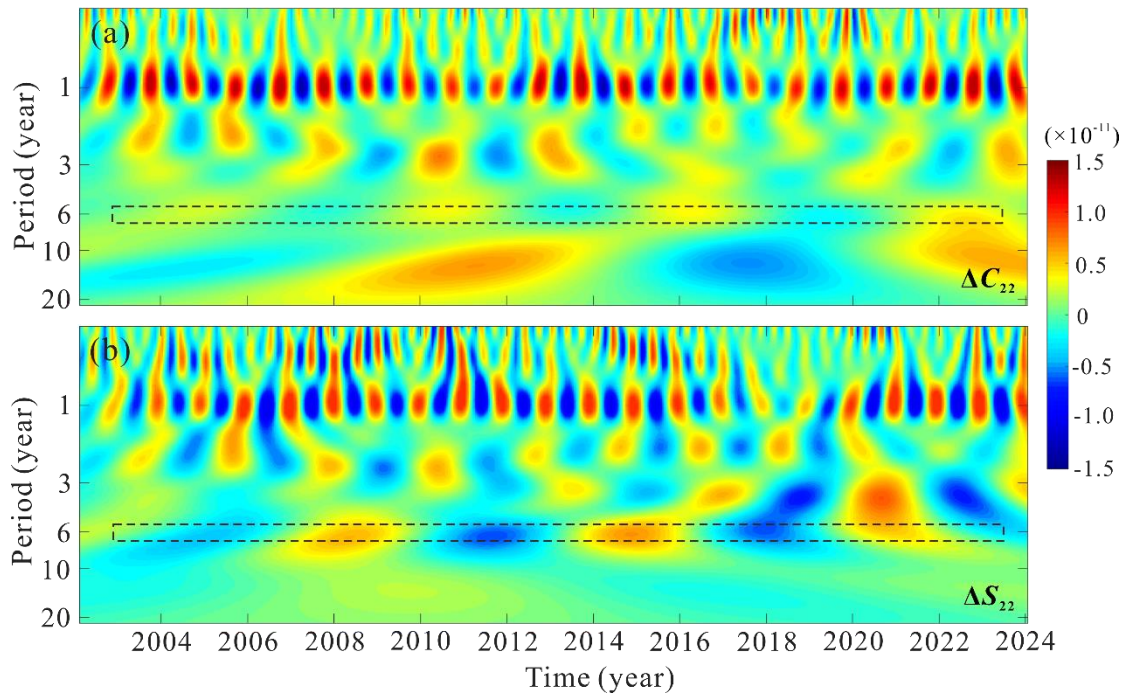


Supplementary Fig. 1 Length-of-day variation (ΔLOD) from observation and external source excitations and corresponding Fourier spectra. (a) Length-of-day variation (ΔLOD) observation with their corresponding excited results by the atmospheric, oceanic (OAM), and hydrologic angular momentum (AAM, OAM, and HAM), respectively. (b) Fourier amplitude spectra of the ΔLOD observation, corresponding excited results by the AAM and OAM (AAM+OAM; AO) and HAM, and the residual sequence of ΔLOD observation minus AAM and OAM ($\Delta\text{LOD-AO}$).

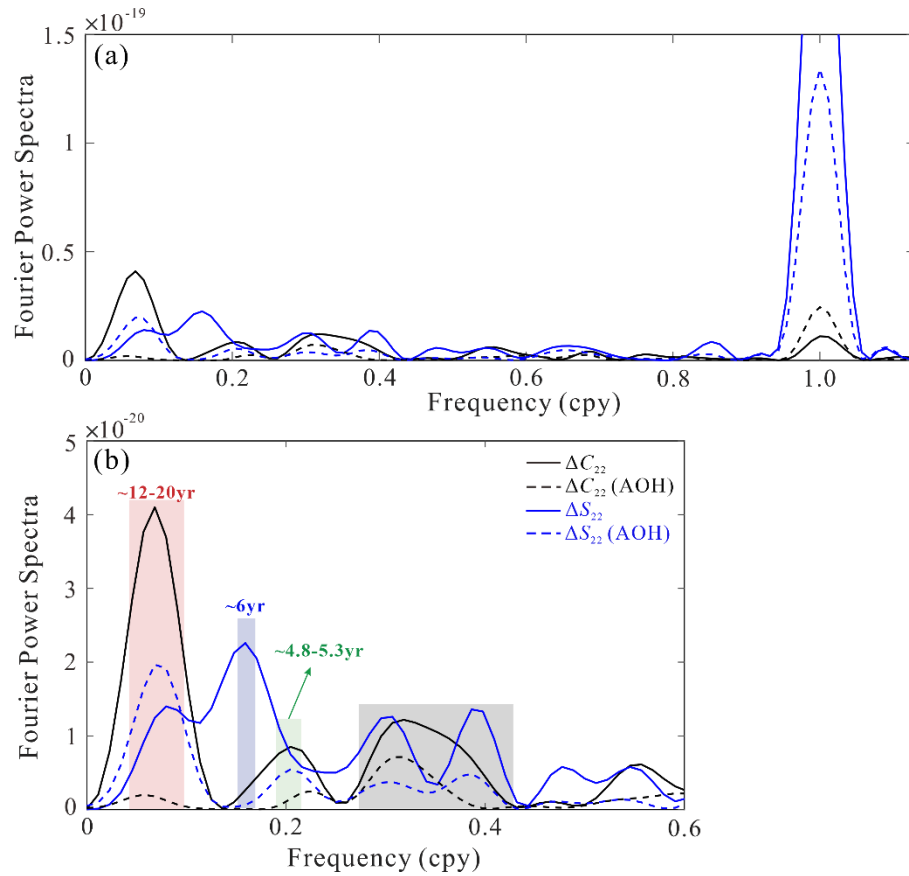
Spectra of the degree-2 order-2 gravitational Stokes coefficients

To verify the detection results in Fig. 3, we conducted further analysis using wavelet spectra to assess the stability of signals detected in the degree-2 order-2 gravitational Stokes coefficients ΔS_{22} and ΔC_{22} datasets, as shown in Supplementary Fig. 2. In the band with a period of 5-20 years, only one stable and statistically significant signal is discernible in ΔS_{22} , whose period corresponds to ~ 6 -year. Conversely, the signal observed in ΔC_{22} is notably weaker and less stable around the 6-year, manifesting a period shorter than 6 years and denoting a period of the ~ 5.3 -year, as described in the Main text. In addition, ΔC_{22} appears to display a longer period oscillation, but the corresponding period is sharp time-varying and hence is not a stable signal. Moreover, we present the Fourier power spectra of the degree-2 order-2 Stokes

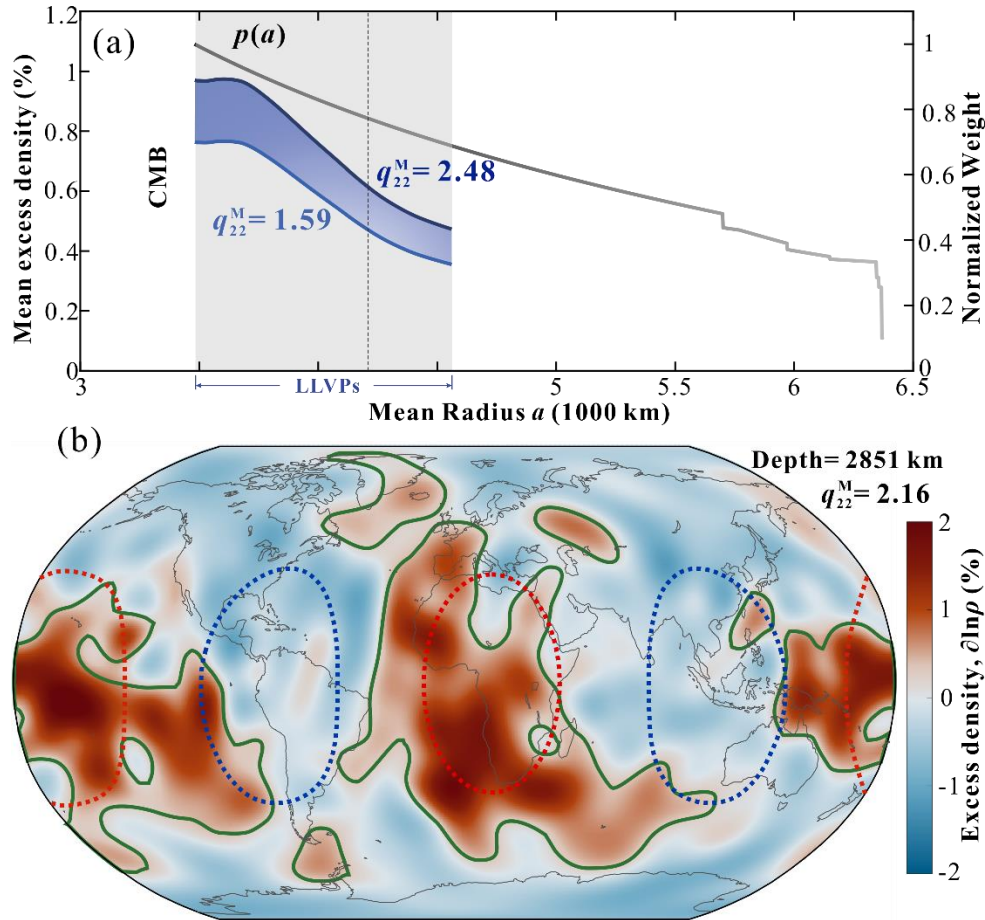
coefficients ΔC_{22} and ΔS_{22} observations, as well as those influenced by external sources (i.e., atmospheric, oceanic, and hydrological effects; AOH) in Supplementary Fig. 3. Notably, Supplementary Fig. 3 exhibits four prominent peaks in the observed ΔS_{22} and three prominent peaks in the observed ΔC_{22} , distinctly revealing a ~ 5 -year cycle instead of a ~ 6 -year cycle in ΔC_{22} . Corresponding signals can also be identified in external sources, except for the ~ 6 -year oscillation in ΔS_{22} . Based on this analysis, we conclude that the ΔS_{22} only exhibits one signal on the intradecadal scale, corresponding to a period of ~ 6 years, with no signal of the same period found in external sources. Conversely, the signal of a similar period in ΔC_{22} corresponds to ~ 5 -year, also appearing in external sources and indicating that it may stem from residual errors in external modeling.



Supplementary Fig. 2 Wavelet spectra of the degree-2 order-2 gravitational Stokes coefficients that atmospheric, oceanic and hydrologic effects have been removed. (a) Corresponding the coefficient ΔC_{22} . (b) Corresponding the coefficient ΔS_{22} .



Supplementary Fig. 3 The Fourier power spectra of raw data from satellite laser (SLR) ranging products of CSR and external excitations for the $\Delta C_{22}/\Delta S_{22}$. (a) Fourier power spectra of the degree-2 order-2 Stokes coefficients ΔC_{22} and ΔS_{22} observations, as well as those influenced by external sources (atmospheric, oceanic, and hydrologic effects; AOH). (b) is an enlarged view of the 0-0.6 cpy band of (a).



Supplementary Fig. 4 Inversion of the density anomaly of the large low-velocity provinces (LLVPs) based the S362MANI model. (a) Normalized weight function $p(a)$ (gray curve) and the mean radius-dependent mean density anomaly range of the LLVPs below the radius (blue shaded area); the gray shaded area indicates the LLVPs location range. (b) The excess density $\partial \ln \rho$ (in %) converted by the S362MANI model at the depth of 2851 km is based on the mantle's interior multipole 2.16 (corresponding to MICG torque of 4.0×10^{20} N·m; Buffett & Mound, 2005); the green curves circle the contour of the LLVPs defined by the $-6.5\text{‰}V_s$ (Karato et al., 1993; Lau et al., 2017; Richards et al., 2023); the dashed curves circle the sensitive region of degree-2 order-2 density multipoles and different colors mean they have opposite symbols.

References

- Braginsky, S. I. (1998). Magnetic Rossby waves in the stratified ocean of the core, and topographic core-mantle coupling. *Earth, planets and space*, 50(8), 641-649.
- Braginsky, S. I. (1999). Dynamics of the stably stratified ocean at the top of the core. *Physics of the earth and planetary interiors*, 111(1-2), 21-34.

- Buffett, B. A. (1996a). Gravitational oscillations in the length of day. *Geophysical Research Letters*, 23(17), 2279-2282.
- Buffett, B. A. (1996b). A mechanism for decade fluctuations in the length of day. *Geophysical research letters*, 23(25), 3803-3806.
- Buffett, B. A. (1997). Geodynamic estimates of the viscosity of the Earth's inner core. *Nature*, 388(6642), 571-573.
- Buffett, B. A. (2014). Geomagnetic fluctuations reveal stable stratification at the top of the Earth's core. *Nature*, 507(7493), 484-487.
- Buffett, B. A., & Mound, J. E. (2005). A Green's function for the excitation of torsional oscillations in the Earth's core. *Journal of Geophysical Research: Solid Earth*, 110(B8).
- Chao, B. F. (2017a). Dynamics of axial torsional libration under the mantle-inner core gravitational interaction. *Journal of Geophysical Research: Solid Earth*, 122(1), 560-571.
- Chao, B. F. (2017b). Dynamics of the inner core wobble under mantle-inner core gravitational interactions. *Journal of Geophysical Research: Solid Earth*, 122(9), 7437-7448.
- Cheng, M., & Ries, J. (2023). C_{20} and C_{30} variations from SLR for GRACE/GRACE-FO science applications. *Journal of Geophysical Research: Solid Earth*, 128(2), e2022JB025459.
- Ciufolini, I., Paolozzi, A., Pavlis, E. C., Sindoni, G., Koenig, R., Ries, J. C., ... & Paris, C. (2017). A new laser-ranged satellite for General Relativity and space geodesy:

- I. An introduction to the LARES2 space experiment. *The European Physical Journal Plus*, 132, 1-9.
- Conrad, C. P., Steinberger, B., & Torsvik, T. H. (2013). Stability of active mantle upwelling revealed by net characteristics of plate tectonics. *Nature*, 498(7455), 479-482.
- Creager, K. C. (1997). Inner core rotation rate from small-scale heterogeneity and time-varying travel times. *Science*, 278(5341), 1284-1288.
- Davies, C. J., Stegman, D. R., & Dumberry, M. (2014). The strength of gravitational core-mantle coupling. *Geophysical Research Letters*, 41(11), 3786-3792.
- Dehant, V., Campuzano, S. A., De Santis, A., & van Westrenen, W. (2022). Structure, materials and processes in the Earth's core and mantle. *Surveys in Geophysics*, 43(1), 263-302.
- Deuss, A. (2014). Heterogeneity and anisotropy of Earth's inner core. *Annual Review of Earth and Planetary Sciences*, 42, 103-126.
- Ding, H. (2019). Attenuation and excitation of the ~ 6 year oscillation in the length-of-day variation. *Earth and Planetary Science Letters*, 507, 131-139.
- Ding, H., & Chao, B. F. (2018). Application of stabilized AR-z spectrum in harmonic analysis for geophysics. *Journal of Geophysical Research: Solid Earth*, 123(9), 8249-8259.
- Ding, H., Pan, Y., Xu, X. Y., Shen, W., & Li, M. (2019). Application of the AR-z spectrum to polar motion: A possible first detection of the inner core wobble and its implications for the density of Earth's core. *Geophysical Research Letters*,

46(23), 13765-13774.

Dumberry, M. (2008). Decadal variations in gravity caused by a tilt of the inner core.

Geophysical Journal International, 172(3), 921-933.

Dumberry, M., & Manda, M. (2022). Gravity variations and ground deformations resulting from core dynamics. *Surveys in Geophysics*, 1-35.

Dziewonski, A. M., & Anderson, D. L. (1981). Preliminary reference Earth model.

Physics of the earth and planetary interiors, 25(4), 297-356.

Forte, A. M., Woodward, R. L., & Dziewonski, A. M. (1994). Joint inversions of seismic and geodynamic data for models of three—dimensional mantle heterogeneity. *Journal of Geophysical Research: Solid Earth*, 99(B11), 21857-21877.

Gross, R. S. (2007). Earth rotation variations-long period. *Treatise on geophysics*, 3(821), 239-294.

Gubbins, D. (1981). Rotation of the inner core. *Journal of Geophysical Research: Solid Earth*, 86(B12), 11695-11699.

Holme, R., & De Viron, O. (2013). Characterization and implications of intradecadal variations in length of day. *Nature*, 499(7457), 202-204.

Karato, S. I. (1993). Importance of anelasticity in the interpretation of seismic tomography. *Geophysical research letters*, 20(15), 1623-1626.

Koelemeijer, P., Deuss, A., & Ritsema, J. (2017). Density structure of Earth's lowermost mantle from Stoneley mode splitting observations. *Nature Communications*, 8(1), 15241.

- Kustowski, B., Ekström, G., & Dziewoński, A. M. (2008). Anisotropic shear-wave velocity structure of the Earth's mantle: A global model. *Journal of Geophysical Research: Solid Earth*, *113*(B6).
- Laske, G., & Masters, G. (1999). Limits on differential rotation of the inner core from an analysis of the Earth's free oscillations. *Nature*, *402*(6757), 66-69.
- Laske, G., Masters, G., Ma, Z., & Pasyanos, M. (2013, April). Update on CRUST1. 0—A 1-degree global model of Earth's crust. In *Geophysical research abstracts* (Vol. 15, No. 15, p. 2658).
- Lau, H. C., Mitrovica, J. X., Davis, J. L., Tromp, J., Yang, H. Y., & Al-Attar, D. (2017). Tidal tomography constrains Earth's deep-mantle buoyancy. *Nature*, *551*(7680), 321-326.
- Mound, J. E., & Buffett, B. A. (2003). Interannual oscillations in length of day: Implications for the structure of the mantle and core. *Journal of Geophysical Research: Solid Earth*, *108*(B7).
- Mound, J. E., & Buffett, B. A. (2006). Detection of a gravitational oscillation in length-of-day. *Earth and Planetary Science Letters*, *243*(3-4), 383-389.
- Petit, G., Luzum, B., & Bureau International Des Poids Et Mesures Sevres (France). (2010). IERS Conventions (2010).
- Ray, R. D., & Erofeeva, S. Y. (2014). Long-period tidal variations in the length of day. *Journal of Geophysical Research: Solid Earth*, *119*(2), 1498-1509.
- Richards, F. D., Hoggard, M. J., Ghelichkhan, S., Koelemeijer, P., & Lau, H. C. (2023). Geodynamic, geodetic, and seismic constraints favour deflated and dense-cored

LLVPs. *Earth and Planetary Science Letters*, 602, 117964.

Ritsema, J., Deuss, A., Van Heijst, H. J., & Woodhouse, J. H. (2011). S40RTS: a degree-40 shear-velocity model for the mantle from new Rayleigh wave dispersion, teleseismic traveltimes and normal-mode splitting function measurements. *Geophysical Journal International*, 184(3), 1223-1236.

Rochester, M. G., Crossley, D. J., & Chao, B. F. (2018). On the physics of the inner-core wobble; corrections to “dynamics of the inner-core wobble under mantle-inner-core gravitational interactions” by BF Chao. *Journal of Geophysical Research: Solid Earth*, 123(11), 9998-10.

Song, X., & Richards, P. G. (1996). Seismological evidence for differential rotation of the Earth's inner core. *Nature*, 382(6588), 221-224.

Tkalčić, H. (2024). On the inner-core differential-rotation (un) resolvability from earthquake doublets: The traps of data selection. *Geophysical Research Letters*, 51(6), e2023GL107043.

Tkalčić, H., Young, M., Bodin, T., Ngo, S., & Sambridge, M. (2013). The shuffling rotation of the Earth's inner core revealed by earthquake doublets. *Nature Geoscience*, 6(6), 497-502.

Vidale, J. E., Dodge, D. A., & Earle, P. S. (2000). Slow differential rotation of the Earth's inner core indicated by temporal changes in scattering. *Nature*, 405(6785), 445-448.

Wang, W., & Vidale, J. E. (2022). Seismological observation of Earth's oscillating inner core. *Science Advances*, 8(23), eabm9916.

Wen, L. (2006). Localized temporal change of the Earth's inner core boundary. *Science*, 314(5801), 967-970.

Yang, Y., & Song, X. (2023). Multidecadal variation of the Earth's inner-core rotation. *Nature Geoscience*, 16(2), 182-187.

Yuan, Q., Li, M., Desch, S. J., Ko, B., Deng, H., Garnero, E. J., ... & Asimow, P. D. (2023). Moon-forming impactor as a source of Earth's basal mantle anomalies. *Nature*, 623(7985), 95-99.

Zhang, W., & Shen, W. (2020). New estimation of triaxial three-layered Earth's inertia tensor and solutions of Earth rotation normal modes. *Geodesy and Geodynamics*, 11(5), 307-315.

Data availability

The Δ LOD and external sources datasets used in this work are available via IERS (<https://www.iers.org/IERS/EN/DataProducts/EarthOrientationData/eop.html>). The degree-2 order-2 gravitational field Stokes coefficients measured by the SLR are from https://filedrop.csr.utexas.edu/pub/slr/degree_2/C22_S22_RL06.txt. The mantle's speed models S40RTS and S362MANI are respectively from [SubMachine: Web-based tools for exploring seismic tomography and other models of Earth's deep interior \(ox.ac.uk\)](#) and [SAGE: Data Services Products: EMC-S362ANI+M \(iris.edu\)](#).